

EVALUATION OF PIXEL SELECTION METHODS FOR TRAFFIC INFRASTRUCTURE MONITORING USING SENTINEL-1 INSAR

A. Piter^{1,*}, M. H. Haghighi¹, M. Motagh^{1,2}

¹ Institute of Photogrammetry and GeoInformation, Leibniz Universität Hannover, Germany - (piter, mahmud)@ipi.uni-hannover.de

²GFZ German Research Centre for Geosciences, Section of Remote Sensing and Geoinformatics, 14473 Potsdam, Germany
motagh@gfz-potsdam.de

KEY WORDS: InSAR, traffic infrastructure, monitoring, Persistent Scatterer Interferometry, Phase-Linking.

ABSTRACT:

The Synthetic Aperture Radar (SAR) satellite Sentinel-1 provides excellent traffic infrastructure monitoring capabilities due to its short revisit time, wide-scale coverage and free of charge data policy. However, pixels from Sentinel-1 have a medium spatial resolution so that traffic infrastructure is only covered by a few pixels. Moreover, Interferometric Synthetic Aperture Radar (InSAR) yields deformation time series for coherent pixels only, thus limiting the number of pixels reporting the ground motion at traffic infrastructure. Although various InSAR time series methods have been successfully applied for traffic infrastructure monitoring, the selection of appropriate methods achieving a high pixel density has not yet been evaluated. In this study, we test whether we can improve the monitoring capabilities by combining different InSAR time series methods. On the one hand, we applied widely used Stanford Method for Persistent Scatterers (StaMPS) as a baseline method to retrieve the deformation time series. On the other hand, we enhanced the phase quality in a pre-processing step using the Phase-Linking (PL) approach and afterwards estimated the deformation time series also with StaMPS based on pixels selected by PL. We compared and evaluated the achieved pixel densities from both methods at main roads, highways and railways in a study area in Germany. We found that the InSAR time series methods selected complementary sets of pixels at all traffic infrastructure types. Moreover, the results indicate a great potential for railway monitoring using Sentinel-1 InSAR due to both high pixel density and homogeneous spatial distribution of pixels. Interestingly, coherent scatterers selected by StaMPS were observed to coincide with large traffic signs at highways which show a double-bounce scattering in the amplitude images. This study shows the benefits of combining PL and StaMPS for increased pixel density at traffic infrastructure and confirms Sentinel-1 data as a suitable data source for traffic infrastructure monitoring.

1. INTRODUCTION

Today's society depends on highly connected and intact traffic infrastructure. Every day, freight and passengers are transported on the road and rail networks. However, traffic infrastructure might get damaged, e.g., due to the ageing process or ground motion induced by natural and anthropogenic processes. Monitoring the ground motion at traffic infrastructure is an important geodetic task which helps in preventing damage or even the collapse of the infrastructure (Shamshiri et al., 2014). While conventional geodetic techniques like levelling and GNSS measurements merely achieve a limited spatial coverage, spaceborne Interferometric Synthetic Aperture Radar (InSAR) is a well-established method to assess ground motion over wide areas with a millimeter to centimeter accuracy (Bürgmann et al., 2000).

The suitability of InSAR for monitoring task was shown by region-wide (Del Soldato et al., 2019), nation-wide (Kalia et al., 2017; Dehls et al., 2019; Papoutsis et al., 2020; Bakon et al., 2020; Bischoff et al., 2020) and European-wide (Crosetto et al., 2020) ground motion services. Country and continental-scale ground motion services deliver valuable information, but the InSAR processing chain in such services is not optimized for specific tasks such as traffic infrastructure monitoring (Haghighi and Motagh, 2017, 2021). Moreover, ground motion services have long update intervals, thus specific InSAR time series processing is needed to evaluate current conditions regarding stability of infrastructure.

In the Netherlands, ground motion was monitored with InSAR nation-wide at railway tracks (Chang et al., 2016). Images from the C-band Synthetic Aperture Radar (SAR) satellite Radarsat-2 were processed with Delft Persistent Scatterer Interferometry (DePSI) to derive ground displacements. In that context, sensitivity and quality metrics were derived for multi-satellite constellations (Chang et al., 2018). They illustrate the potential and the limitations of InSAR for railway monitoring depending on the viewing direction of the satellites with respect to the direction of the railway tracks.

The SAR satellite Sentinel-1 launched in 2014, became a game-changer for InSAR monitoring applications. Sentinel-1 carries a C-band sensor, has a short repetition interval of 6 days and the data is free of charge, which makes it an excellent choice for InSAR time series analysis and monitoring tasks. However, linear traffic features like highways, railways and bridges are difficult to monitor with Sentinel-1, because their spatial extent is small compared to the spatial resolution of a Sentinel-1 pixel (North et al., 2017; Chang et al., 2020). Sentinel-1 provides medium resolution images of roughly 5m×20m in range and azimuth, respectively. Hence, a 6-lane highway, for instance, is covered by 5-6 Sentinel-1 pixels in range and by 1-2 pixels in azimuth depending on the direction of the highway with respect to the satellite's viewing direction. Main roads are even smaller and often only covered by 1-2 Sentinel-1 pixels in range. In addition to the low number of Sentinel-1 pixels covering traffic infrastructure, the number of pixels for which the deformation can be estimated reliably with InSAR is further reduced due to decorrelation of the signal. InSAR time series analysis relies on pixels with a coherent backscattering signal over time

* Corresponding author

and preferably with a low phase noise. On the one hand, effort is needed to select as many coherent scatterers on the traffic infrastructure as possible to accurately assess the deformation behaviour. On the other hand, incoherent pixels have to be discarded to avoid the propagation of errors during unwrapping of the interferometric phase.

Data from Sentinel-1 has been successfully used for traffic infrastructure monitoring with Persistent Scatterer Interferometry (PSI), for instance at the highway network of Rome (Orellana et al., 2020), at the highspeed railway bridge in Nanjing (Huang et al., 2017, 2018) and for studying the relation to soil movement in the United Kingdom (North et al., 2017). However, these studies discussed neither the sufficiency of the achieved density of coherent pixels nor the optimal choice of InSAR time series method for traffic infrastructure monitoring.

The challenge of reaching a sufficient pixel density in the area of interest was addressed by Chang and Hanssen (2015) for deformation monitoring at the Qinghai–Tibet railway. In order to increase the pixel density, they created a buffer around the railway tracks and estimated the coherence per pixel. A spatially adaptive filter based on statistically homogeneous pixels (SHP) (Ferretti et al., 2011) was applied to provide a better estimate of the coherence per pixel compared to the boxcar filter. Qin et al. (2019) also addressed the achievable pixel density and combined coherent pixels from PSI with less coherent pixels using a Small Baseline Subset (SBAS) network of interferograms with relaxed thresholds on the pixel's coherence.

Two types of physical scattering mechanisms are commonly distinguished in SAR images: distributed scatterers (DS) and persistent scatterers (PS) (Hanssen, 2001).

For pixels with a distributed scattering mechanism the signal is the sum of the reflected signals from several objects within the SAR resolution cell, where no single scatterer is dominating. Distributed scatterers (DS) follow a complex-valued gaussian distribution and the phase noise can be described by coherence. DS are prone to various sources of decorrelation and often exhibit a low signal-to-noise ratio (SNR) compared to persistent scatterers (PS). DS are often related to natural objects and rural areas. An improvement of the SNR of DS is necessary for InSAR time series analysis. In the SBAS method, multilooking increases the SNR, but reduces the spatial resolution. This approach is not suitable for deformation monitoring at traffic infrastructure using Sentinel-1 images, because the highest possible spatial resolution is required.

Point-like scattering is the second scattering type, more often referred to as persistent scatterers. The total signal of PS is dominated by the signal from a single object in the SAR resolution cell and consists of a constant signal plus noise. The coherence of PS remains high independent from the interferometric baseline configuration, which makes it possible to use even interferograms with large temporal baselines for displacement analysis. PS are often related to man-made structures.

There is lack of knowledge about the prevalent scattering mechanisms and their characteristics at traffic infrastructure. This knowledge is needed to select an appropriate InSAR time series method to achieve a high density of coherent scatterers. A high density and homogeneous distribution of coherent pixels is required to reliably assess and monitor ground deformation at traffic infrastructure. In this work, we analyse the challenges and opportunities of traffic infrastructure monitoring using InSAR time series analysis with medium spatial resolution

Sentinel-1 images. We therefore investigate the prevalent scattering mechanisms based on intermediate results from Phase-Linking (PL). Our aim is to increase the pixel density by combining different InSAR time series methods for the selection of coherent pixels on traffic infrastructure. To that end, we focus on the combination of PL with Stanford Method for Persistent Scatterers (StaMPS) to achieve a high pixel density. We compare the set of selected pixels from both methods to examine whether selected pixels are redundant. In this work, we distinguish between incoherent and coherent DS, and between incoherent point-like scatterers and coherent point-like scatterers which we call PS. The combined set of coherent DS and PS are summarized by the term coherent scatterers.

The remainder of this paper is structured as follows. In section 2 we present the InSAR time series methods with their pixel selection strategy which were used to investigate the achievable pixel density at traffic infrastructure from Sentinel-1 data. In section 3 we evaluate the pixel selection methods based on experiments in a study area in Germany. In section 4 we conclude our findings and give an outlook to ensuing work.

2. METHODOLOGY

2.1 Interferometric Synthetic Aperture Radar

InSAR measures the wrapped phase difference between two SAR acquisitions imaging the same spatial extent on the Earth's surface. The phase difference can be due to different components: ground deformation, different atmospheric effects at the time of the acquisitions, flat Earth, topography, and noise. To retrieve the ground deformation, all other components have to be either removed or neglected and the interferometric phase needs to be unwrapped. InSAR time series methods improve the removal of the unwanted components by using a network of interferograms. Unwrapping the interferometric phase is challenging, especially when the phase noise is high. Therefore, pixels with low phase noise need to be selected by InSAR time series methods prior to unwrapping.

InSAR time series methods differ, amongst others, by the type of scatterers they address. The methods have in common that they identify pixels with reliable phase, regardless of scattering type. They perform unwrapping and time series analysis on the selected pixels. Further, all InSAR time series methods infer the displacement time series by resolving the atmospheric signal and the remaining topographic signal from a stack of interferograms. In the following, two well-known time series methods that are applied on full resolution are reviewed.

2.2 Persistent Scatterer Interferometry

PSI addresses the characteristics of PS by a single-reference network of interferograms (Ferretti et al., 2001). Importantly, PSI is applied on full resolution interferograms due to the high SNR of PS pixels. PSI can reveal deformation signals present in single pixels only. While PSI methods mainly select PS at man-made objects by thresholding on amplitude dispersion (Ferretti et al., 2001; Kampes, 2006), Stanford Method for Persistent Scatterers (StaMPS) is designed to also select PS from natural objects that exhibit a low amplitude (Hooper et al., 2007). StaMPS selects PS pixels which have a low phase noise in a single-reference network of interferograms. The pixels selected by StaMPS are therefore not restricted to point-like scatterers. Pixels with a distributed scattering mechanism which do not decorrelate due to long temporal or perpendicular baselines might also have a low phase noise and be identified by StaMPS.

The pixel selection is done with iterative spatiotemporal filtering. Hereby, all phase contributions are removed based on assumptions about correlation in time and/or space, such that only the phase noise remains. As an advantage, StaMPS does not require any assumptions about deformation behaviour. Once all pixels with a low phase noise are selected, the phase time series is unwrapped in time and space. At the end, the temporal coherence is used to describe the phase noise and to select high quality pixels after InSAR time series analysis (Ferretti et al., 2001).

2.3 Phase-Linking

Phase-Linking (PL) addresses the characteristics of DS. PL overcomes the problem of decorrelation of DS by enhancing the SNR (Guarnieri and Tebaldini, 2008; Ferretti et al., 2011). In contrast to conventional SBAS which uses multilooking to enhance the SNR, PL retains the full spatial resolution of the interferograms. After PL, DS and PS can be jointly processed using any InSAR method to retrieve the deformation signal. PL consists of a non-linear phase inversion of all possible interferograms in three steps. First, an adaptive spatial filter is applied on the Single Look Complex (SLC) images to find pixels that share the same backscattering mechanism, so-called statistically homogeneous pixels (SHP). The number of SHP is used to distinguish pixels with distributed from pixels with point scattering mechanism. Based on findings from Ferretti et al. (2011), pixels with equal or more than 20 SHP are classified as DS. In the second step, only the identified DS are considered further. For each of the DS, the complex coherence matrix is computed from the complex-valued backscattering time series of its SHP. In the third step, the non-linear phase inversion is performed based on the coherence matrix. Hereby, the quality of the phase time series is improved. The success of PL and, hence, the resulting quality of the DS phase time series is evaluated for each pixel by the PL coherence (Ferretti et al., 2011). Pixels with a high PL coherence are thereafter exploited in the same way as PS. It was shown for various applications that PL increases the pixel density compared to PSI only, e.g. for landslide monitoring (Mirzaee et al., 2017), for monitoring of cavern-related ground subsidence (Even et al., 2020) and city subsidence in Mexico City (Osmanoğlu et al., 2016). The higher pixel density reveals more detailed information about the displacement and its distribution.

3. EXPERIMENTS

3.1 Study area and dataset

We exemplarily investigate the pixel selection on traffic infrastructure in a study area close to Cologne in mid-west Germany. In the Rhenish coal fields, brown coal is produced in three open pit mines: Gazweiler, Inden and Hambach. Ground subsidence due to the mining activities have been studied in detail using InSAR for the period June 2017 to October 2018 (Tang et al., 2020). Time series analysis of Sentinel-1 and TerraSAR-X using the SBAS approach showed maximum displacement rates at e.g. the Hambach open pit mine of up to 50 cm/year in direction of the satellite line-of-sight (LOS). Also neighbouring cities and traffic infrastructure are affected by ground deformations.

The study area is shown in Figure 1 with the traffic infrastructure types which are analysed in our study: railway tracks, highway A4 and A61, and main roads. Furthermore, the subset

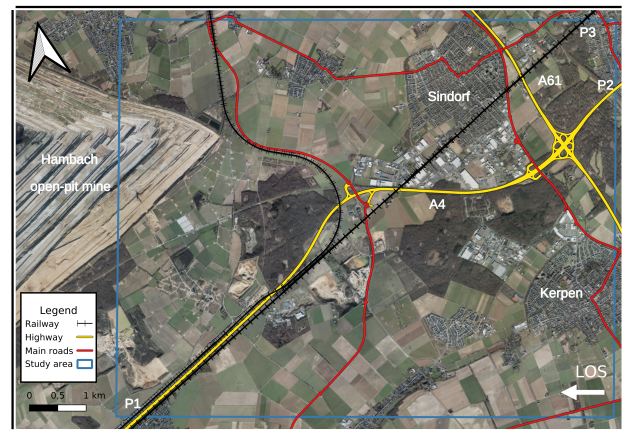


Figure 1. Study area next to Hambach open-pit mine in Germany with the investigated traffic infrastructure highlighted: main roads, highways, railways (OpenStreetMap contributors, 2022). Start and end points of the profiles shown in Figure 4 and 7 are denoted by P1-P3. For highway, the profile is from P1 to P2 and for railway from P1 to P3. Background image: WMS Nordrhein-Westfalen DOP (2021).

of the Sentinel-1 descending track 37 is highlighted. We selected 122 SLC images covering the time span of two years from 2017-03-26 to 2019-03-28. Only a small area was considered for the case study to limit the computation time of the PL processing.

3.2 Experimental setup

The Sentinel-1 SLC images were co-registered to a common reference image (2018-03-27) and interferograms were generated using the open-source software InSAR Computing Environment (ISCE) (Rosen et al., 2012; Fattahi et al., 2017). We used a 30 m resolution digital elevation model (DEM) from Shuttle Radar Topography Mission (SRTM) for DEM-assisted coregistration and to remove the topography component from the interferograms. We then applied two InSAR time series methods. On the one hand, we used StaMPS based on the interferogram stack. On the other hand, we applied PL on the SLC stack, created interferograms from the modified SLCs and transferred them to StaMPS for unwrapping. We used the open-source software Miami NOn linear phase linking in PYthon (MiNoPy) for PL and therefore, in this paper the latter InSAR time series method is termed MiNoPy2StaMPS. To ensure the comparability of the results, we computed for both methods the temporal coherence from the phase residuals after removal of all phase components in StaMPS. Pixels with a temporal coherence lower than 0.8 were discarded.

3.2.1 StaMPS

We estimated the deformation time series for coherent scatterers using the open-source software StaMPS. A single-reference network of interferograms was created using ISCE from the stack of coregistered SLCs. Using StaMPS, pixels with low phase noise were selected, their phase time series were unwrapped in time and space, and the deformation parameters were estimated. The phase quality of the selected pixels was described by the temporal coherence.

3.2.2 MiNoPy2StaMPS

We improved the SNR of DS pixels using the open-source software MiNoPy (Mirzaee and Amelung, 2018; Mirzaee et

al., 2019). SHP were detected based on the two sample t-test (Shamshiri et al., 2018) in a 19×9 neighbourhood in range \times azimuth, respectively. We classified pixels with equal or more than 20 SHP as DS. Pixels with less than 20 SHP are referred to as non-DS. We did not apply PL for non-DS and therefore did not investigate these pixels. The coherence matrices per pixel were computed from its SHP and the optimal phase time series were inferred with Eigendecomposition-based Maximum-likelihood estimator of Interferometric phase (EMI) (Ansari et al., 2018). To reduce the computational burden, the sequential EMI estimator (Ansari et al., 2017) was applied with a ministack size consisting of 30 images each. The PL coherence was used to extract coherent DS from the set of DS. Pixels with a PL coherence equal or greater than 0.8 are considered to have a high phase quality and hence, to be coherent. For coherent DS, the deformation time series was estimated using StaMPS from a single-reference network of interferograms which was created using ISCE. To ensure that all coherent DS are included, we skipped the pixel selection step in StaMPS and processed all selected coherent DS.

3.2.3 Extracting the area of interest

After InSAR time series analysis, the selected pixels from both methods were intersected with a spatial mask to extract only pixels related to traffic infrastructure. The mask was created from OpenStreetMap vector data (OpenStreetMap contributors, 2022) for three types of traffic infrastructure: main roads, highways and railway tracks (cf. Figure 1). The spatial mask was created from lines with a width of 3 pixels for main roads, 6 pixels for highways and 2 pixels per railway track.

3.3 Results and discussion

We compare the results from StaMPS and MiNoPy2StaMPS only for the masked traffic infrastructure pixels. First, the distribution of DS is analysed based on the results from MiNoPy2StaMPS. Second, pixel densities from both methods along the traffic infrastructures are analysed. Third, a pixel-wise comparison of selected pixels from both methods is given. Finally, the estimated deformation map and mean deformation profiles from both methods are discussed.

3.3.1 Analysis of distributed scatterers

Figure 2 shows the number of pixels covering the traffic infrastructure types. In the study area, most of the pixels covering traffic infrastructure are related to highways, followed by railways and the least pixels are on main roads. For each traffic infrastructure type the number of identified DS is shown. All traffic infrastructure types have in common that the majority of pixels show a distributed scattering mechanism. For railways, the percentage of DS compared to non-DS is the lowest with roughly 60 %, while for highways the percentage is the highest with about 70 %.

Furthermore, the amount of selected coherent DS are shown per traffic infrastructure type. The highest percentage of coherent DS is found at railways and the lowest at main roads.

The number of coherent DS depends on the chosen threshold for the PL coherence. To maximize the number of selected coherent DS, lower thresholds are desirable. However, a low threshold comes at the cost of including more incoherent pixels. The cumulative distribution of the PL coherence is shown in Figure 3. It can be seen that more DS on railways have a high coherence compared to highways and main roads. The curves from railways and highways are similar for coherence values

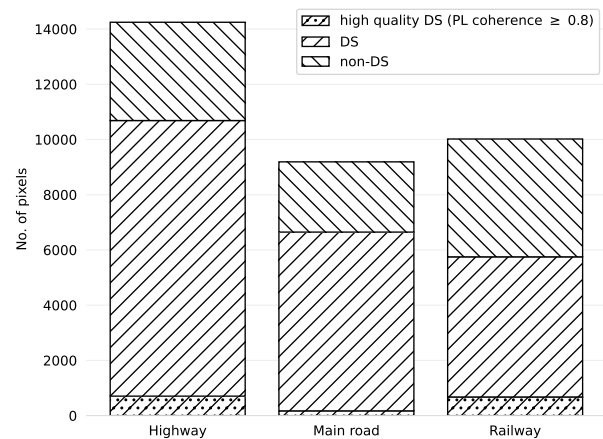


Figure 2. Comparison of the absolute distribution of identified DS and coherent DS based on thresholding the number of SHP and thresholding the PL coherence, respectively, for three traffic infrastructure types.

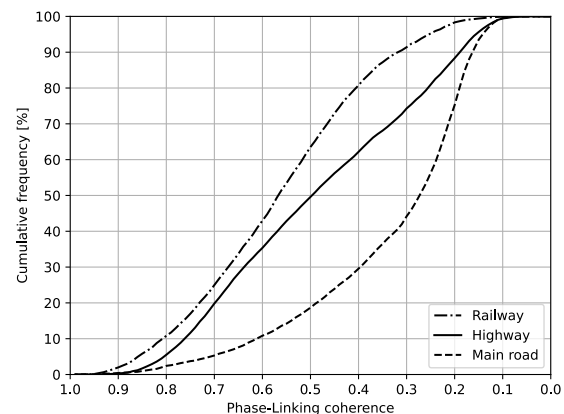


Figure 3. Cumulative distributions of the PL coherence for DS pixels per traffic infrastructure type.

between 0.6 and 1.0, but show higher differences for lower values. About 10% of the DS at railways have a coherence higher than 0.8, while it is only roughly 5% at highways. By lowering the threshold for the PL coherence from 0.8 to 0.7, 25% of the DS at railways and 20% at highways would be included. For main roads, the distribution is considerably worse. The curve shows a different distribution compared to railways and highways with only 20% of the DS having a PL coherence higher than 0.5. Lowering the threshold from 0.8 to 0.7 would include 5% of the DS instead of roughly 3%. Hence, the number of exploitable DS at main roads is much lower than at railways and highways.

The differences in the distribution may arise from different surface roughness. Possibly, a rough surface of gravel and railway ties in the resolution cell of a pixel leads to a better backscattering signal. The road surfaces scatter most of the signal away from the satellite and appear dark in SAR images. However, the coherence distributions also differ among the highway and main roads. Probably the spatial extend of the traffic infrastructure within the coverage of a pixel plays a role.

Interestingly, the visual inspection of the SHP location revealed that the spatial distribution of the SHP often follows the shape

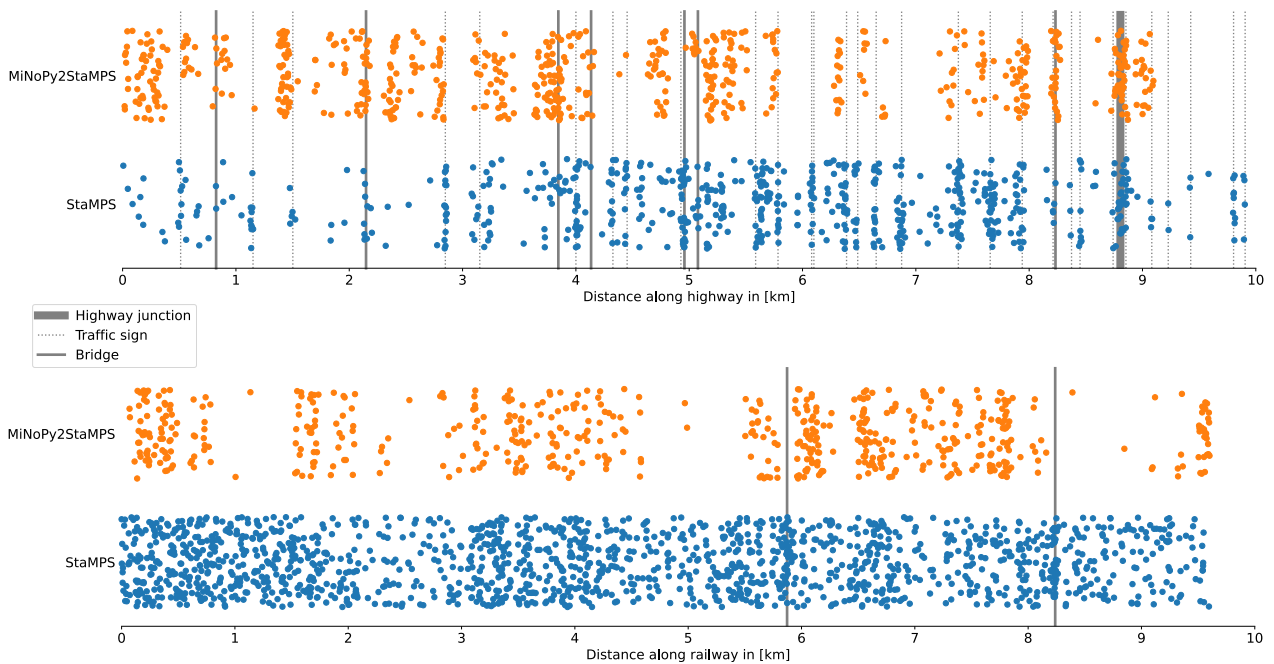


Figure 4. Distribution of selected pixels from StaMPS and MiNoPy2StaMPS along the highway A4 from P1 to P2 (top) and railway from P1 to P3 (bottom) (cf. Figure 1). Points are located randomly along the y-axis for improved readability of the figure.

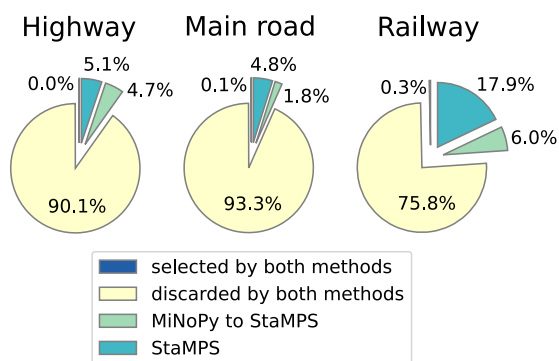


Figure 5. Comparison of selected pixels from StaMPS and MiNoPy2StaMPS at the traffic infrastructures.

of the traffic infrastructure. This shows that DS on the traffic infrastructure are scattering similarly to each other and differently compared to the surrounding. The surrounding is often covered by vegetation and, hence, it is incoherent. When considering the spatial extend of main roads compared to the size of the Sentinel-1 pixels, it becomes clear that not many pixels within the considered spatial neighbourhood cover the main road as well. Therefore, if a pixel from a main road shows a distributed scattering, the corresponding SHP might probably be related to the surrounding, which often is vegetation in rural areas or buildings in urban areas. This could be an explanation for the worse PL coherence distribution at main roads.

3.3.2 Analysis of pixel densities

In the following, we compare the selected pixels from StaMPS and MiNoPy2StaMPS.

To assess the pixel density, we determined the position of the selected pixels along the traffic infrastructure relative to a starting point. Figure 4 (top) exemplarily shows the location of selected

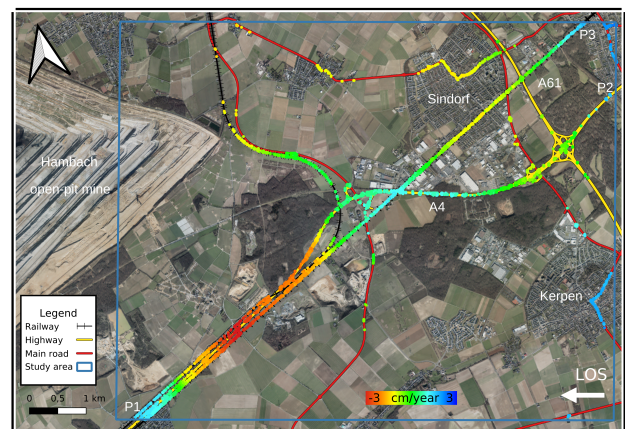


Figure 6. Mean deformation velocities in the study area shown for the traffic infrastructure only. Pixels from both StaMPS and MiNoPy2StaMPS are shown together.

coherent scatterers at the highway A4. The scatterers are shown along the highway from the points P1 to P2 which are depicted in Figure 1. Along the y-axis, the points are scattered by a uniformly distributed random value to avoid overlapping of pixels which have a similar distance along the highway. The highway is covered irregularly by pixels from both methods. The location of the pixels along the highway is different for the pixels selected from StaMPS and MiNoPy2StaMPS. For instance at 1.5 km and 2.4 km only MiNoPy2StaMPS and similarly, at 4.2 km and 6.1 km only StaMPS selects pixels. This shows that the two methods select complementary sets of pixels at highways. Moreover, pixels from StaMPS appear to be spatially clustered. For example, a higher pixel density was found at the A4-A61 highway junction. Moreover, we observed the coincidence of the selected pixels with the location of large traffic signs along the highway. Therefore, we included the location

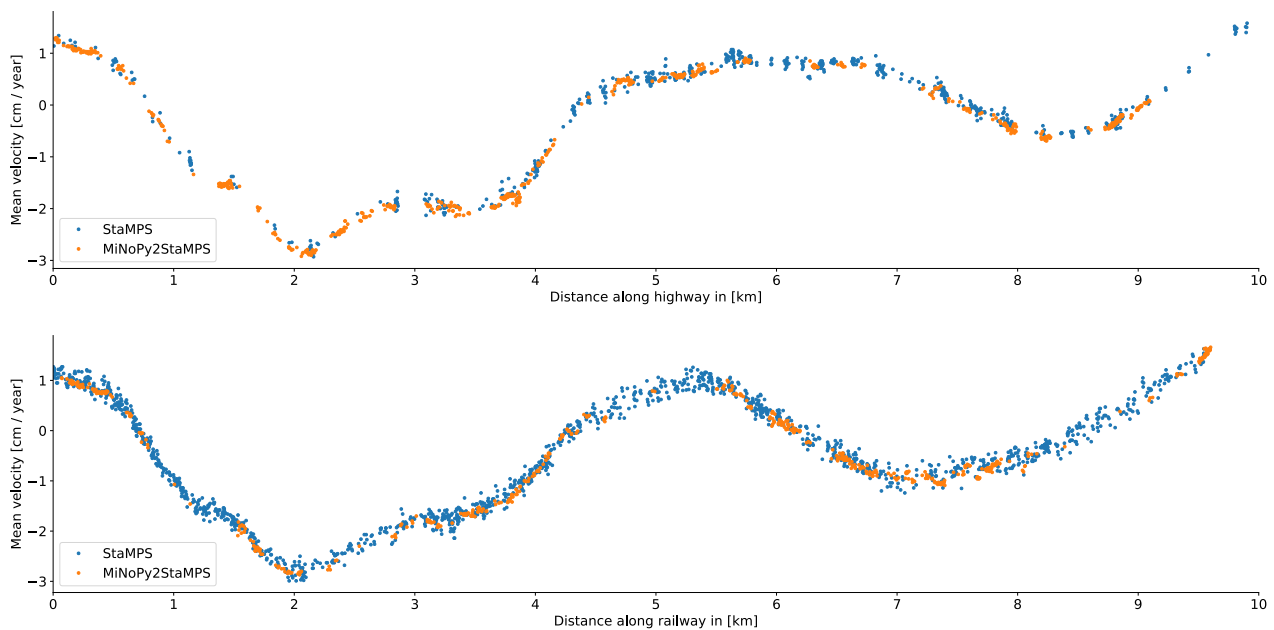


Figure 7. Profiles of mean deformation velocity in LOS along the highway A4 from P1 to P2 (top) and railway from P1 to P3 (bottom) (cf. Figure 1) derived with StaMPS and MiNoPy2StaMPS.

of large traffic signs, bridges and the highway junction into the figure. The coincidence with large traffic signs appears mostly for pixels selected by StaMPS. With MiNoPy2StaMPS, pixels are selected without relation to large traffic signs. The analysis of the SAR amplitude time series revealed high backscattering signals at large traffic signs. Hence, a double-bounce at the large traffic signs is likely the reason for the good phase quality. Figure 4 (bottom) shows the spatial distribution of coherent scatterers along the railway exemplarily for the section from P1 to P3 (cf. Figure 1). A high and homogeneous pixel density was achieved by StaMPS, while the distribution is much sparse from MiNoPy2StaMPS. At roughly 5.8 km and 8.3 km the higher densities of pixels from StaMPS were found to coincide with the bridges of highways A4 and A61, respectively. Further correlation of groups of coherent pixels with a particular surrounding were not found.

At main roads the pixel density was found to be low in the whole study area. The selected pixels from both methods are mostly located within urban areas, that suggests the backscattered signal might not originate from the main road itself but from double bounce at surrounding buildings. The density of the selected pixels is insufficient to retrieve and monitor displacements at main roads outside urban areas independent of the method.

3.3.3 Comparison of selected pixels

The pixel densities along the traffic infrastructures differ for StaMPS and MiNoPy2StaMPS results. However, the spatial distribution does not reveal differences in the pixel selection on the basis of individual pixels. In the following, we directly compare the pixels selected from both methods.

Figure 5 shows the percentage of pixels selected per traffic infrastructure type in four categories: Pixels selected by both methods, discarded by both methods, selected only by StaMPS and selected only by MiNoPy2StaMPS. The percentages per category are similar for each of the traffic infrastructures. Most of the pixels were discarded by both StaMPS and MiNoPy2StaMPS, while only below one percent of the pixels

were selected by both methods. The percentage of pixels being selected by only StaMPS is higher than the percentage of pixels selected only by MiNoPy2StaMPS. Interestingly, the percentage of discarded pixels is lower for railways than for highways and main roads. For railways, almost 25% of all pixels were selected as coherent scatterers, while it is below 10% for both highways and main roads. The results imply that StaMPS and MiNoPy2StaMPS select different sets of pixels and complement each other. Hence, InSAR time series analysis for traffic infrastructure monitoring benefits from the combination of both methods. Noteworthy, the results indicate high monitoring potential using Sentinel-1 InSAR for railways.

3.3.4 Comparison of estimated deformation parameters

The deformation map in Figure 6 shows the mean deformation velocities in the study area at the traffic infrastructures. Here, the pixels from both methods are shown together. The results from the methods match well and show the same deformation behaviour along both highway and railway. Figure 7 depicts the mean deformation velocity along the highway (top) and railway (bottom) (similar to Figure 4). The mean deformation velocities estimated from StaMPS and from MiNoPy2StaMPS are shown and range from -3 cm/year to 1.5 cm/year in the satellite LOS. The displacement behaviour is revealed at the whole railway while some gaps are visible along the highway. Nevertheless, combining pixels from StaMPS and MiNoPy2StaMPS yields a complementing impression of the displacement at the highway.

4. CONCLUSION

In this study, we evaluated pixel selection methods for InSAR-based traffic infrastructure monitoring using Sentinel-1 images which have a medium spatial resolution. We investigated the prevalence of distributed and point-like scattering at traffic infrastructures and tested whether StaMPS and PL yield different sets of selected pixels. For this purpose, three traffic infrastructure types were analysed: main roads, highways and railways.

We found that distributed scattering is the more frequent scattering mechanism prevalent at traffic infrastructure in our study area. The pixel-wise comparison of the selected pixels from StaMPS and MiNoPy2StaMPS revealed two complementary sets of pixels with low redundancy. This means that although StaMPS already selects coherent scatterers in a single-reference network of interferograms, a combination with PL is beneficial and increases the pixel density. The comparison among the traffic infrastructure types indicated that the monitoring potential using Sentinel-1 InSAR is highest for railways. Precisely, railways were covered by the highest density and a spatially homogeneous distribution of coherent scatterers. At highways, the results revealed an irregular pixel density and, interestingly, we observed a correlation between PS occurrence and the location of large traffic signs which show a double-bounce scattering. We found an insufficient pixel density at main roads possibly resulting from its small spatial extent compared to the size of a Sentinel-1 pixel. Moreover, our results showed that a slight change in the threshold on PL coherence can significantly increase the DS density at railways and highways, while the increase is only small at main roads.

One limitation of our study is the small study area which was chosen to limit the computational burden from PL. Future work should therefore include larger study areas and different ascending and descending tracks to investigate the influence of incidence angle and direction of the traffic infrastructure with respect to the satellite's viewing direction.

Although our results show almost no redundancy among the results from both methods, further work is needed to investigate the influence of the chosen network of interferograms on the pixel selection in StaMPS. We recommend the comparison of our results with the pixel selection of StaMPS with an SBAS network of interferograms.

This study adds to the understanding of traffic infrastructure monitoring using Sentinel-1 InSAR and provides an empirical basis for the selection of appropriate InSAR time series methods.

ACKNOWLEDGEMENTS

This work is part of the project SAR4Infra funded by the German Federal Ministry for Digital and Transport (BMDV). It contains modified Copernicus data provided by the European Space Agency (ESA). Maps and profiles were created with QGIS (QGIS Development Team, 2021).

REFERENCES

Ansari, H., De Zan, F., Bamler, R., 2017. Sequential Estimator: Toward Efficient InSAR Time Series Analysis. *IEEE Transactions on Geoscience and Remote Sensing*, 55(10), 5637–5652.

Ansari, H., De Zan, F., Bamler, R., 2018. Distributed scatterer interferometry tailored to the analysis of big InSAR data. *EU-SAR 2018; 12th European Conference on Synthetic Aperture Radar*, VDE, 1–5.

Bakon, M., Czikhart, R., Papco, J., Barlak, J., Rovnak, M., Adamisin, P., Perissin, D., 2020. remotIO: A Sentinel-1 Multi-Temporal InSAR Infrastructure Monitoring Service with Automatic Updates and Data Mining Capabilities. *Remote Sensing*, 12(11), 1892.

Bischoff, C. A., Ferretti, A., Novali, F., Uttini, A., Giannico, C., Meloni, F., 2020. Nationwide deformation monitoring with

SqueeSAR® using Sentinel-1 data. *Proceedings of the International Association of Hydrological Sciences*, 382, 31–37.

Bürgmann, R., Rosen, P. A., Fielding, E. J., 2000. Synthetic Aperture Radar Interferometry to Measure Earth's Surface Topography and Its Deformation. *Annual Review of Earth and Planetary Sciences*, 28(1), 169–209.

Chang, L., Dollevoet, R. P., Hanssen, R. F., 2016. Nationwide railway monitoring using satellite SAR interferometry. *IEEE Journal of Selected Topics in Applied Earth Observations and Remote Sensing*, 10(2), 596–604.

Chang, L., Dollevoet, R. P., Hanssen, R. F., 2018. Monitoring line-infrastructure with multisensor SAR interferometry: Products and performance assessment metrics. *IEEE Journal of Selected Topics in Applied Earth Observations and Remote Sensing*, 11(5), 1593–1605.

Chang, L., Hanssen, R., 2015. Detection of permafrost sensitivity of the Qinghai–Tibet railway using satellite radar interferometry. *International Journal of Remote Sensing*, 36(3), 691–700.

Chang, L., Sakpal, N. P., Elberink, S. O., Wang, H., 2020. Railway Infrastructure Classification and Instability Identification Using Sentinel-1 SAR and Laser Scanning Data. *Sensors*, 20(24), 7108.

Crosetto, M., Solari, L., Mróz, M., Balasis-Levinsen, J., Casagli, N., Frei, M., Oyen, A., Moldestad, D. A., Bateson, L., Guerrieri, L., Comerci, V., Andersen, H. S., 2020. The Evolution of Wide-Area DInSAR: From Regional and National Services to the European Ground Motion Service. *Remote Sensing*, 12(12), 2043.

Dehls, J. F., Larsen, Y., Marinkovic, P., Lauknes, T. R., Stødle, D., Moldestad, D. A., 2019. INSAR.No: A National InSAR Deformation Mapping/Monitoring Service In Norway – From Concept To Operations. *IGARSS 2019 - 2019 IEEE International Geoscience and Remote Sensing Symposium*, 5461–5464. ISSN: 2153-7003.

Del Soldato, M., Solari, L., Raspini, F., Bianchini, S., Ciampalini, A., Montalti, R., Ferretti, A., Pellegrineschi, V., Casagli, N., 2019. Monitoring Ground Instabilities Using SAR Satellite Data: A Practical Approach. *ISPRS International Journal of Geo-Information*, 8(7), 307.

Even, M., Westerhaus, M., Simon, V., 2020. Complex Surface Displacements above the Storage Cavern Field at Epe, NW-Germany, Observed by Multi-Temporal SAR-Interferometry. *Remote Sensing*, 12(20), 3348.

Fattahi, H., Agram, P., Simons, M., 2017. A network-based enhanced spectral diversity approach for TOPS time-series analysis. *IEEE Transactions on Geoscience and Remote Sensing*, 55(2), 777–786.

Ferretti, A., Fumagalli, A., Novali, F., Prati, C., Rocca, F., Rucci, A., 2011. A new algorithm for processing interferometric data-stacks: SqueeSAR. *IEEE Transactions on Geoscience and Remote Sensing*, 49(9), 3460–3470.

Ferretti, A., Prati, C., Rocca, F., 2001. Permanent scatterers in SAR interferometry. *IEEE Transactions on Geoscience and Remote Sensing*, 39(1), 8–20.

- Guarnieri, A. M., Tebaldini, S., 2008. On the exploitation of target statistics for SAR interferometry applications. *IEEE Transactions on Geoscience and Remote Sensing*, 46(11), 3436–3443.
- Haghighi, M. H., Motagh, M., 2017. Sentinel-1 InSAR over Germany: Large-scale interferometry, atmospheric effects, and ground deformation mapping. *ZfV: Zeitschrift für Geodäsie, Geoinformation und Landmanagement*, 2017(4), 245–256.
- Haghighi, M. H., Motagh, M., 2021. Land Subsidence Hazard in Iran Revealed by Country-Scale Analysis of Sentinel-1 InSAR. *The International Archives of Photogrammetry, Remote Sensing and Spatial Information Sciences*, XLIII-B3-2021, 155–161.
- Hanssen, R. F., 2001. *Radar interferometry: data interpretation and error analysis*. 2, Springer Science & Business Media.
- Hooper, A., Segall, P., Zebker, H., 2007. Persistent scatterer interferometric synthetic aperture radar for crustal deformation analysis, with application to Volcán Alcedo, Galápagos. *Journal of Geophysical Research: Solid Earth*, 112(B7).
- Huang, Q., Crosetto, M., Monserrat, O., Crippa, B., 2017. Displacement monitoring and modelling of a high-speed railway bridge using C-band Sentinel-1 data. *ISPRS Journal of Photogrammetry and Remote Sensing*, 128, 204–211.
- Huang, Q., Monserrat, O., Crosetto, M., Crippa, B., Wang, Y., Jiang, J., Ding, Y., 2018. Displacement monitoring and health evaluation of two bridges using Sentinel-1 SAR images. *Remote Sensing*, 10(11), 1714.
- Kalia, A. C., Frei, M., Lege, T., 2017. A Copernicus downstream-service for the nationwide monitoring of surface displacements in Germany. *Remote Sensing of Environment*, 202, 234–249.
- Kampes, B. M., 2006. *Radar interferometry*. 12, Springer.
- Mirzaee, S., Amelung, F., 2018. Volcanic Activity Change Detection Using SqueeSAR-InSAR and Backscatter Analysis. 2018, G41B–0707.
- Mirzaee, S., Amelung, F., Fattahi, H., 2019. Non-linear phase inversion package for time series analysis. 2019, G13C–0572.
- Mirzaee, S., Motagh, M., Akbari, B., Wetzel, H. U., Roessner, S., 2017. Evaluating Three InSAR Time-Series Methods to Assess Creep Motion, Case Study: Masouleh Landslide in North Iran. *ISPRS Annals of Photogrammetry, Remote Sensing and Spatial Information Sciences*, 41W1, 223–228.
- North, M., Farewell, T., Hallett, S., Bertelle, A., 2017. Monitoring the response of roads and railways to seasonal soil movement with Persistent Scatterers Interferometry over six UK sites. *Remote Sensing*, 9(9), 922.
- OpenStreetMap contributors, 2022. OpenStreetMap. <https://www.openstreetmap.org>.
- Orellana, F., Delgado Blasco, J. M., Foumelis, M., D'Aranno, P. J., Marsella, M. A., Di Mascio, P., 2020. DInSAR for Road Infrastructure Monitoring: Case Study Highway Network of Rome Metropolitan (Italy). *Remote Sensing*, 12(22), 3697.
- Osmanoğlu, B., Sunar, F., Wdowinski, S., Cabral-Cano, E., 2016. Time series analysis of InSAR data: Methods and trends. *ISPRS Journal of Photogrammetry and Remote Sensing*, 115, 90–102.
- Papoutsis, I., Kontoes, C., Alatza, S., Apostolakis, A., Loupasakis, C., 2020. InSAR Greece with Parallelized Persistent Scatterer Interferometry: A National Ground Motion Service for Big Copernicus Sentinel-1 Data. *Remote Sensing*, 12(19), 3207.
- QGIS Development Team, 2021. QGIS Geographic Information System. Open Source Geospatial Foundation. <http://qgis.osgeo.org>.
- Qin, X., Ding, X., Liao, M., Zhang, L., Wang, C., 2019. A bridge-tailored multi-temporal DInSAR approach for remote exploration of deformation characteristics and mechanisms of complexly structured bridges. *ISPRS Journal of Photogrammetry and Remote Sensing*, 156, 27–50.
- Rosen, P. A., Gurrola, E., Sacco, G. F., Zebker, H., 2012. The InSAR scientific computing environment. *EUSAR 2012; 9th European Conference on Synthetic Aperture Radar*, VDE, 730–733.
- Shamshiri, R., Motagh, M., Baes, M., Sharifi, M. A., 2014. Deformation analysis of the Lake Urmia causeway (LUC) embankments in northwest Iran: insights from multi-sensor interferometry synthetic aperture radar (InSAR) data and finite element modeling (FEM). *Journal of Geodesy*, 88(12), 1171–1185.
- Shamshiri, R., Nahavandchi, H., Motagh, M., Hooper, A., 2018. Efficient ground surface displacement monitoring using Sentinel-1 data: Integrating distributed scatterers (DS) identified using two-sample t-test with persistent scatterers (PS). *Remote Sensing*, 10(5), 794.
- Tang, W., Motagh, M., Zhan, W., 2020. Monitoring active open-pit mine stability in the Rhenish coalfields of Germany using a coherence-based SBAS method. *International Journal of Applied Earth Observation and Geoinformation*, 93, 102217.